Simultaneous retrievals of column ozone and aerosol optical properties from direct and diffuse solar irradiance measurements

Christian D. Goering,[1] Tristan S. L'Ecuyer,[1] Graeme L. Stephens,[1] James R. Slusser,[2] Gwen Scott,[2] John Davis,[2] James C. Barnard,[3] and Sasha Madronich[4]

Received 9 August 2004; revised 23 November 2004; accepted 17 December 2004; published 11 March 2005.

[1] A retrieval technique has been developed to simultaneously determine column ozone amounts and aerosol optical properties using surface observations of solar ultraviolet direct normal and diffuse horizontal irradiance from a multifilter rotating shadowband radiometer. The retrieval consists of a Bayesian scheme involving a tropospheric ultraviolet radiative transfer model. The technique was tested using cloud-free observations collected during a Mexico City Metropolitan Area air pollution field campaign from April to May 2003. Retrieval results compared favorably to those of independent techniques, including ozone amounts from a direct-Sun method, Langley-derived aerosol optical depths, and aerosol single-scattering albedos from a direct-to-diffuse irradiance ratio technique. Further comparisons were performed between the measurements and model simulations when using the retrieval results as inputs, both from the proposed technique and the combined independent methods. Simulations using the results of the new method were found to agree with the observations within the assumed limits of measurement and model uncertainty. It is anticipated that the technique will be applied across a 33-site network of radiometers maintained by the U.S. Department of Agriculture UV-B Monitoring and Research Program for development of aerosol climatologies and for providing ground validation for satellite measurements.

Citation: Goering, C. D., T. S. L'Ecuyer, G. L. Stephens, J. R. Slusser, G. Scott, J. Davis, J. C. Barnard, and S. Madronich (2005), Simultaneous retrievals of column ozone and aerosol optical properties from direct and diffuse solar irradiance measurements, *J. Geophys. Res.*, *110*, D05204, doi:10.1029/2004JD005330.

1. Introduction

[2] Ultraviolet radiation, though less than 7% of the radiant energy emitted by the Sun, greatly impacts the Earth by initiating chemical photolysis and by affecting animals and plants [*Cullen et al.*, 1992; *Madronich*, 1992, 1993; *Gao et al.*, 2002; *Zheng et al.*, 2002]. Only a few mechanisms exist to regulate the amount of UV reaching the earth's surface. One of these is ozone, which absorbs most of the UV radiation shorter than 320 nm in the stratosphere [*Seinfeld and Pandis*, 1998]. However, despite its benefits at high altitude, ozone in the troposphere is considered a pollutant because of the health risks it poses and its ability to damage ecosystems [*McKee*, 1994; *Environment Canada*, 1999]. Because the rate of its production depends on the concentrations of precursors such as nitrogen oxides and nonmethane hydrocarbons, ground-level ozone (photochemical smog) is often associated with urban transportation and industry [*Environment Canada*, 1999; *Dickerson et al.*, 1997].

[3] Atmospheric aerosols also help to regulate UV by absorption and scattering. Although partially introduced into the atmosphere by natural processes, high concentrations of aerosols are often formed in urban areas, where industrial combustion processes and vehicular emissions dominate [*Seinfeld and Pandis*, 1998; *Liou*, 2002]. Urban aerosols are in particular recognized for reducing visibility and causing a number of health problems [*Dockery and Pope*, 1994; *Krewski et al.*, 2003].

[4] In nations such as the United States and Canada, federal regulations exist for controlling harmful emissions and reducing air pollution. However, recent research suggests that emission control strategies may result in unintended effects, such as increasing surface UV if ozone-absorbing precursors are reduced in areas where they are highly concentrated [*Castro et al.*, 2001; *Dickerson et al.*, 1997]. This, in turn, may enhance photolysis of remaining concentrations of those same precursors and lead to an increase in photochemical smog. The implication is that, while emission control measures are needed, care must be taken in drafting air pollution regulations, and as such, continued research into the interaction of ultraviolet radiation, aerosols, and ozone is necessary.

[1]Department of Atmospheric Science, Colorado State University, Fort Collins, Colorado, USA.
[2]U.S. Department of Agriculture UV-B Monitoring and Research Program, Natural Resource Ecology Laboratory, Colorado State University, Fort Collins, Colorado, USA.
[3]Pacific Northwest National Laboratory, Richland, Washington, USA.
[4]Atmospheric Chemistry Division, National Center For Atmospheric Research, Boulder, Colorado, USA.

0148-0227/05/2004JD005330$09.00

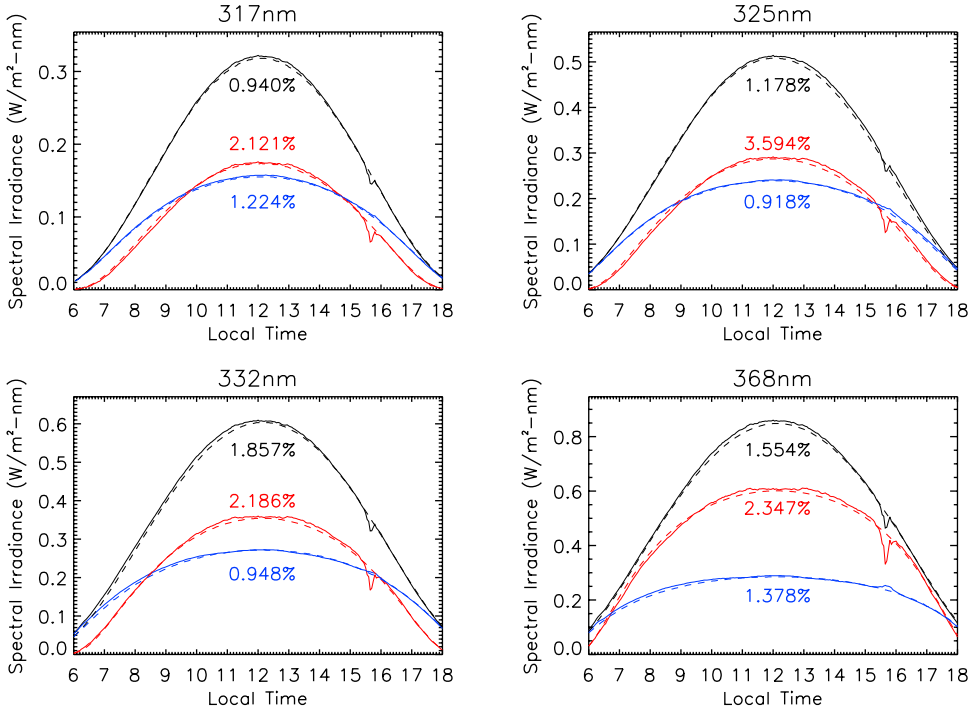

Figure 1. Comparison of observed and model-simulated total horizontal (black), direct normal (red), and diffuse horizontal (blue) irradiances at Davis, California, on 12 May 2003. Solid lines represent observations, dashed lines represent simulated components, and numerical labels indicate the median percentage difference of the simulations relative to the observations.

[5] Because of the high level of air pollution known to exist in the Mexico City metropolitan area (MCMA), in 2003, Drs. Mario and Luisa Molina of the Massachusetts Institute of Technology (MIT) organized a field campaign with the intent of providing a scientific basis for new emission control strategies in the MCMA and, more generally, insight into the air quality problem that exists in large urban areas. A timeframe of five weeks in April to early May 2003 was selected to coincide with the period of maximum photochemical activity. A site was designated for immobile, ground-based instruments at the Centro Nacional de Investigación y Capacitación Ambiental (CENICA). Data from this site was supplemented by meteorological and chemical data collected by collaborating Mexican research groups at alternate locations in the city (MCMA-2003 Field Measurement Campaign, available from Massachusetts Institute of Technology Web site at http://eaps.mit.edu/megacities/mcma_fieldcampaign/overview/).

[6] The U.S. Department of Agriculture (USDA) UV-B Monitoring and Research Program (UVMRP) at Colorado State University contributed to the MCMA-2003 field campaign by providing a Yankee Environmental Systems ultraviolet multifilter rotating shadowband radiometer (UV-MFRSR) from its network of ground-based instruments [*Bigelow et al.*, 1998]. Data collected by the instrument was compiled at the UVMRP office during and after the campaign. This paper describes how this data set was subsequently used in developing the optimal estimation technique [*Rodgers*, 2000] for simultaneous retrievals of aerosol optical depth (τ_{aer}) and single-scattering albedo (ω_{aer}) at the 7 nominal wavelengths of the UV-MFRSR, in addition to daily total column ozone amounts, for facilitation of field campaign goals and for future application across the UVMRP network.

[7] It is important to acknowledge that previous research studies have provided a number of individual methods for determining the above parameters of interest. *Shaw et al.* [1973] presented the Langley regression technique for retrieval of τ_{aer} from a multiwavelength direct-Sun pointing radiometer, while *Herman et al.* [1975] introduced the diffuse-to-direct irradiance ratio as a tool to determine the imaginary term in the complex index of refraction. Irradiance ratios have since been used in several studies to determine ω_{aer} in the UV range [*Kylling et al.*, 1998; *Krotkov et al.*, 2003; *Petters et al.*, 2003; *Wetzel et al.*, 2003]. *Wenny et al.* [1998] used forward simulations of UV

Table 1. Numerical Results From the Model Consistency Check at Davis, California

	Passband			
	368 nm	332 nm	325 nm	317 nm
Median difference (total horizontal), %	1.6	1.9	1.2	0.9
Median difference (diffuse horizontal), %	1.4	0.9	0.9	1.2
Median difference (direct horizontal), %	2.3	2.2	3.6	2.1
Difference at solar noon (total horizontal), %	1.3	0.7	0.9	1.0
Difference at solar noon (diffuse horizontal), %	1.4	0.4	0.6	1.4
Difference at solar noon (direct normal), %	1.2	1.2	1.1	0.5

Table 2. Number of Cloud-Screened Measurements and Corresponding Range of Indices for Individual Days During the Field Campaign

Date, 2003	Number of Measurements	Index Range
5 April	49	0–48
6 April	16	49–64
8 April	4	65–68
12 April	21	69–89
14 April	38	90–127
15 April	51	128–178
16 April	65	179–243
17 April	33	244–276
18 April	42	277–318
21 April	15	319–333
24 April	16	334–349
26 April	41	350–390
27 April	23	391–413
30 April	24	414–437
2 May	17	438–454

transmission to determine aerosol optical properties, while *Slusser et al.* [1999] and *Gao et al.* [2001] presented column ozone retrieval techniques specifically for the UV-MFRSR. *Wenny et al.* [2001] retrieved column ozone in addition to τ_{aer} from UV-MFRSR measurements. The intent of this research is not to replace these efforts, but rather to build upon the list of available techniques by providing an advanced retrieval containing a built-in analysis of uncertainty and set of diagnostics while taking the findings of others into account.

[8] In the following section, details are presented pertaining to the data and methods used, including the UV-MFRSR in section 2.1, the tropospheric ultraviolet radiative transfer model in section 2.2, the optimal estimation technique in section 2.3, and the cloud-screening process in section 2.4. Section 3 discusses results from the Mexico City field campaign, including comparisons to TOMS ozone measurements and results from the direct-Sun method [*Gao et al.*, 2001], τ_{aer} determined via Langley regression, and ω_{aer} derived from a direct-to-diffuse irradiance ratio technique. Finally, future improvements to the technique are detailed in section 4.

2. Measurements and Methodology

2.1. Instrumentation and Calibration

[9] As described by *Bigelow et al.* [1998], the UV-MFRSR uses seven independent interference filter photodiode detector combinations and a common diffuser to simultaneously measure total (direct plus diffuse) horizontal irradiance in passbands centered at nominal wavelengths of 300, 305.5, 311.4, 317.6, 325.4, 332.4, and 368 nm. Each has a bandwidth of 2 nm full width at half maximum. A computer-controlled shadowband additionally allows measurement of the diffuse horizontal irradiance, while the direct normal irradiance is derived in near-real time by an onboard processor. Measurements are obtained every 20 s but stored as 3-min averages. Quality assurance of the measurements is achieved through corrections applied as a result of Langley-derived instrument calibration [*Slusser et al.*, 2000], regular evaluation of detector spectral cosine responses, as well as stability and precision studies. As such, UV-MFRSR measurements have been shown to compare quite favorably with those of other ground-based instruments [*Estupiñán et al.*, 2001], in addition to satellite measurements and model simulations [*Slusser et al.*, 2001].

[10] The USDA UVMRP uses Langley calibration coefficients in the form of wavelength-dependent zero-airmass voltage ($V_{0,\lambda}$) both for converting measured voltage (V_λ) to irradiance as well as for routine computations of τ_{aer} and column ozone. For the UV-MFRSR, each $V_{0,\lambda}$ is determined using a Langley Analyzer program that implements the regression algorithm of *Harrison and Michalsky* [1994]. Under ideal conditions, the Langley analysis would produce a $V_{0,\lambda}$ pair for each passband on each day of operation, and these values would be constant. In reality, however, the value of $V_{0,\lambda}$ changes with atmospheric conditions, and the number of values that can be obtained varies greatly from one site to another. Turbid sites, in particular, typically allow for little or no determination of $V_{0,\lambda}$. As such, daily coefficients during the field campaign were estimated from those obtained by the same instrument immediately before and after deployment in the MCMA. Specifically, coefficients were obtained before the campaign at a site in Big Bend, Texas from 1 to 23 February 2003, and afterward at Christman Field in Fort Collins, Colorado from 13 May to 2 June 2003.

[11] Given the determination of daily $V_{0,\lambda}$ coefficients, the UVMRP is able to compute τ_{aer} for an individual UV-MFRSR measurement by first calculating the total (clear-sky) optical depth, given by

$$\tau^* = -(\cos Z)\ln\left(\frac{V_\lambda}{V_{0,\lambda}}\right), \quad (1)$$

where Z represents the solar zenith angle at the time of measurement, and then subtracting contributions to τ^* due to absorption by atmospheric gases (in this case, ozone) and Rayleigh scattering, as parameterized by *Stephens* [1994].

2.2. Radiative Transfer Model

[12] In order to facilitate the retrievals specified in section 1, a tropospheric ultraviolet radiative transfer model (TUV4.2) was chosen as a forward model based on its flexibility and the successful application of a prior version in recent aerosol studies [*Castro et al.*, 2001; *Petters et al.*, 2003; *Wetzel et al.*, 2003]. Among the highlights of this latest version are built-in radiative transfer options that include nine variations on the two-stream approximation [*Toon et al.*, 1989] and a multistream discrete ordinates method [*Stamnes et al.*, 1988]. Additionally, built-in or user-defined physical, biological, and chemical weighting functions, such as instrument response functions and action spectra, may be applied to simulated irradiances and actinic fluxes. Weighting functions for the photolysis of chemical

Table 3. Summary of a Priori Information Used for Optimal Estimation Retrievals[a]

Parameter	Expected Range	Initial Guess in $\mathbf{x_a}$	Variance in $\mathbf{S_a}$
O_3	240–310 DU	275 DU	$(35\ \text{DU}/3)^2$
$\tau_{aer,i}$	0.0–1.6	0.8	$(0.8/3)^2$
$\omega_{aer,i}$	0.7–1.0	0.85	$(0.15/3)^2$

[a]DU is Dobson units.

Table 4. Minimum and Maximum Retrieval Parameters and Uncertainties Corresponding to One Standard Deviation Obtained During the Field Campaign

	Retrieval Parameters		Uncertainty	
Parameter	Minimum	Maximum	Minimum, %	Maximum, %
Column O_3	261.1 DU	298.1 DU	1.3	1.8
τ_{aer}, 300 nm	0.33	1.23	4.3	10.5
τ_{aer}, 305 nm	0.30	1.06	2.8	10.0
τ_{aer}, 311 nm	0.32	1.02	2.0	9.1
τ_{aer}, 317 nm	0.32	0.97	1.8	8.8
τ_{aer}, 325 nm	0.29	0.95	1.8	9.3
τ_{aer}, 332 nm	0.30	0.92	1.8	9.0
τ_{aer}, 368 nm	0.26	0.79	2.0	8.9
ω_{aer}, 300 nm	0.76	0.86	4.4	5.9
ω_{aer}, 305 nm	0.83	0.94	2.8	4.5
ω_{aer}, 311 nm	0.77	0.91	2.1	4.1
ω_{aer}, 317 nm	0.75	0.89	2.0	3.9
ω_{aer}, 325 nm	0.75	0.92	1.9	3.9
ω_{aer}, 332 nm	0.73	0.91	1.8	3.9
ω_{aer}, 368 nm	0.71	0.92	2.0	4.0

species are unique in that they consist of the absorption cross section multiplied by the quantum yield at each defined spectral interval and altitude in the model atmosphere. The model can also be customized through a user interface that allows specification of such items as geographic location and elevation, date and range of time or solar zenith angle, spectral region of interest, radiative transfer method, atmosphere characteristics such as column gas amounts and aerosol or cloud properties, as well as output product type and format. Moreover, subroutines allow for customization of source data for the spectral profile of extraterrestrial irradiance, vertical profile of atmospheric aerosol, and absorption cross sections of atmospheric gases.

[13] A consistency check was performed to ensure that this model would be capable of simulating UV-MFRSR measurements to a desired accuracy in an environment with minimal complexities. To this end, a relatively pollution-free site at Davis, California was chosen from the UVMRP network, where such an instrument is permanently located. Measurements from a predominantly clear day on 12 May 2003 were then compared to simulations from the TUV model. For the sake of simplicity, the exercise was limited to finding a selection of inputs such that, over the course of the day, forward simulations of the irradiance components agreed with UV-MFRSR measurements in the four passbands having the longest nominal wavelengths, where the amount of ozone has little or no effect on the results. Results were considered in agreement if the differences between the actual and simulated measurements did not exceed 2% at solar noon and median differences over the time series did not exceed 5%.

[14] Separate model runs were planned to check the bands individually, each iterating on ω_{aer} while holding all other inputs constant. Among the fixed inputs were τ_{aer} determined at solar noon using the Langley regression method described in section 2.1, a column ozone amount of 353 DU and a surface albedo of 6% based on TOMS measurements, and an asymmetry parameter of 0.55 based on the assumption of an environment free of large, forward scattering aerosols as would be found in heavily polluted regions. In addition, spectral response functions of the instrument at Davis were implemented as physical weighting functions in the model. The eight-stream DISORT radiative transfer algorithm was used to determine the spectral irradiance components, each of which was weighted by the response function in the corresponding passband, integrated over the spectrum, and normalized by the sum of the interval-weighted positive spectral responses. Agreement was reached in all four passbands when the following values of ω_{aer} were used as inputs: 0.957 at 317 nm, 0.924 at 325 nm, 0.881 at 332 nm, and 0.988 at 368 nm. Figure 1 illustrates the precision with which each simulated component conformed to the observations, and numerical results are summarized in Table 1.

2.3. Optimal Estimation Framework

[15] The optimal estimation technique provides an adaptable, diagnostic, multiparameter retrieval framework well suited to problems requiring the simultaneous inversion of a large number of distinct observations in order to obtain a set of retrieval parameters consistent with all of them. Theoretical and mathematical details of the technique are provided by a number of recent studies applying the technique to retrievals of water vapor [*Engelen and Stephens*, 1999],

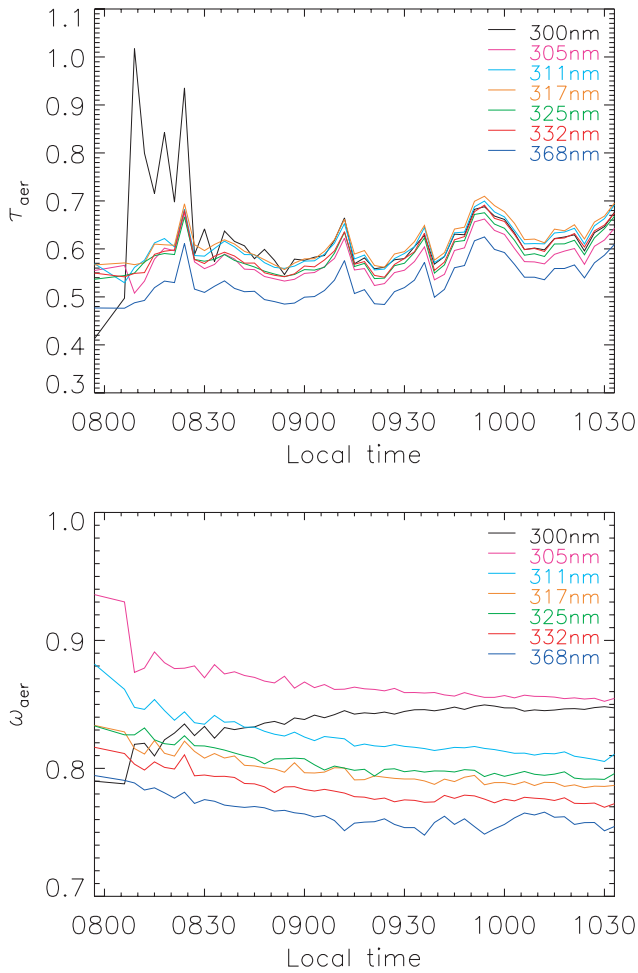

Figure 2. Time series of (top) τ_{aer} and (bottom) ω_{aer} retrieved in each passband for 15 April 2003 using the optimal estimation technique.

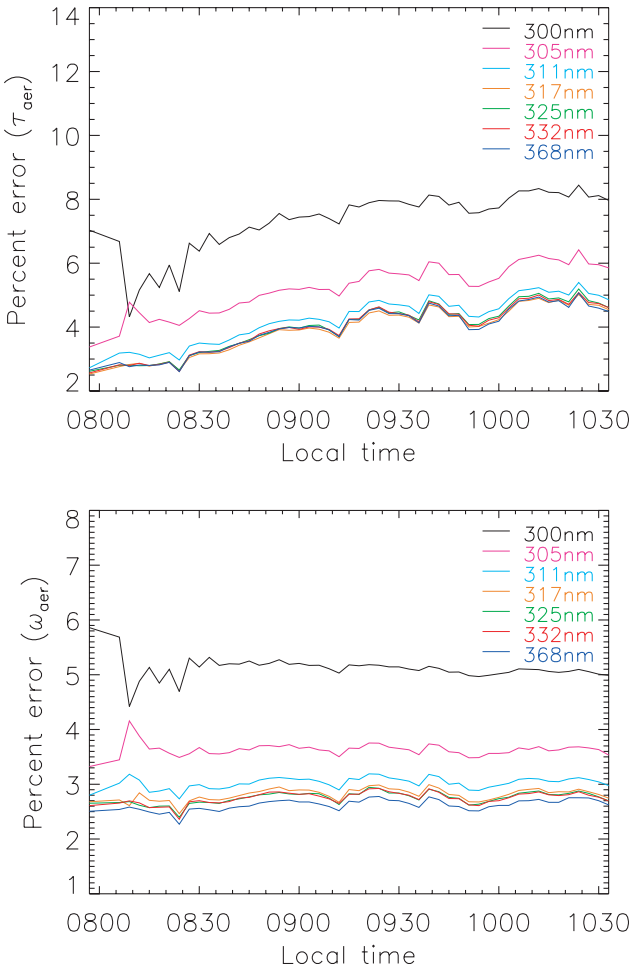

Figure 3. Time series of error percentages corresponding to one standard deviation in (top) τ_{aer} and (bottom) ω_{aer} for 15 April 2003 using the optimal estimation technique.

rainfall [*L'Ecuyer and Stephens*, 2002], and cloud microphysical properties [*Miller et al.*, 2000; *Austin and Stephens*, 2001; *Cooper et al.*, 2003], but are repeated here in the context of retrieving column ozone amounts and aerosol optical properties to simplify interpretation of the results. The set of independent observations corresponding to a single measurement and consisting of direct normal and diffuse horizontal irradiance components are assembled into a measurement vector $\mathbf{y}$, while a state vector $\mathbf{x}$ is defined for the retrieval parameters, consisting of the column ozone amount in addition to τ_{aer} and ω_{aer} at the center wavelength of each passband. The relationship between $\mathbf{x}$ and $\mathbf{y}$ is expressed as

$$\mathbf{y} = F(\mathbf{x}, \mathbf{b}) + \varepsilon, \tag{2}$$

in which F denotes a forward model (in this case, TUV4.2), $\mathbf{b}$ represents a vector of constant model inputs, and ε represents the error involved in mapping model simulations to the observations.

[16] The inversion of (2) is greatly simplified by the assumption that forward model behavior is linear for small perturbations in the state vector. Under this assumption, model behavior is specified in a Jacobian or weighting function matrix $\mathbf{K}$, the elements of which are defined by

$$K_{ij} = \frac{\partial F_i(\mathbf{x})}{\partial x_j} \tag{3}$$

and implemented by using TUV4.2 to compute the change in simulated irradiance components corresponding to a 2% increase in the individual retrieval parameters. (This percentage was chosen based on a model sensitivity study that found only negligible differences in (3) for perturbations of up to 5%.) Applying Bayes' theorem and assuming Gaussian statistics, *Rodgers* [2000] demonstrates that the most probable retrieval solution is that which minimizes the scalar cost function

$$\mathbf{\Phi} = (\mathbf{y} - \mathbf{F}(\hat{\mathbf{x}}))^T \mathbf{S}_\mathbf{y}^{-1} (\mathbf{y} - \mathbf{F}(\hat{\mathbf{x}})) + (\hat{\mathbf{x}} - \mathbf{x_a})^T \mathbf{S}_\mathbf{a}^{-1} (\hat{\mathbf{x}} - \mathbf{x_a}). \tag{4}$$

Specifically, the solution is found by Newtonian iteration via

$$\hat{\mathbf{x}} = \hat{\mathbf{x}}_{i-1} + \hat{\mathbf{S}}\left(\mathbf{K}^T \mathbf{S}_\mathbf{y}^{-1} (\mathbf{y} - \mathbf{F}(\hat{\mathbf{x}}_{i-1})) + \mathbf{S}_\mathbf{a}^{-1} (\mathbf{x_a} - \hat{\mathbf{x}}_{i-1})\right), \tag{5}$$

where

$$\hat{\mathbf{S}} = \left(\mathbf{S}_\mathbf{a}^{-1} + \mathbf{K}^T \mathbf{S}_\mathbf{y}^{-1} \mathbf{K}\right)^{-1} \tag{6}$$

determines the associated retrieval covariance matrix. Here, $\mathbf{x_a}$ represents the best guess of the retrieval parameters prior to the measurement and is termed the a priori state vector. Diagonal elements in covariance matrices $\mathbf{S_a}$ and $\mathbf{S_y}$ specify the uncertainty in the a priori state and combined uncertainty in the measurements and model, respectively, while off-diagonal elements indicate uncertainty correlations between vector elements. The retrieval proceeds until the covariance-weighted square difference between estimates is much less than the number of retrieval parameters (n), as indicated by

$$(\hat{\mathbf{x}} - \hat{\mathbf{x}}_{i-1})^T \hat{\mathbf{S}}^{-1} (\hat{\mathbf{x}} - \hat{\mathbf{x}}_{i-1}) \ll n. \tag{7}$$

[17] Once the solution is determined, the diagonal elements of $\hat{\mathbf{S}}$ provide a direct estimate of the uncertainty in each element of the retrieval vector, defined as

$$e_i = \frac{\sqrt{\hat{S}_{ii}}}{\hat{x}_i} \times 100\% \tag{8}$$

for one standard deviation. Diagonal and off-diagonal elements readily illustrate how the retrieval uncertainty is correlated when used to construct a correlation matrix $\mathbf{C}$ according to

$$Cij = \frac{\hat{S}_{ij}}{\sqrt{\hat{S}_{ii}\hat{S}_{jj}}}. \tag{9}$$

Additional diagnostics provided by the optimal estimation technique further indicate whether the retrieval has worked

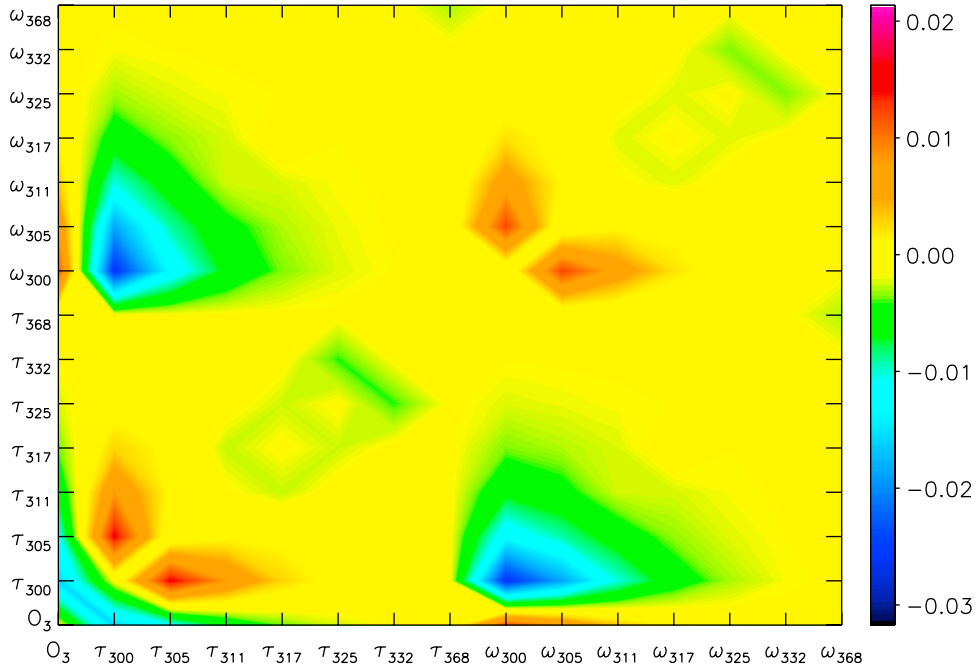

Figure 4. Depiction of the averaged correlation matrix for retrievals on 15 April 2003 with diagonal elements set to zero for greater off-diagonal emphasis.

properly. Most applicable to this research is the averaging kernel matrix defined by

$$\mathbf{A} = \hat{\mathbf{S}}\mathbf{K}^T\mathbf{S}_\mathbf{y}^{-1}\mathbf{K}, \tag{10}$$

which characterizes how the retrieval is resolved. As the accuracy of the retrieval increases, the area encompassed by each row of **A** approaches a value of 1 such that **A** increasingly resembles the identity matrix. Similarity to the identity matrix indicates that the retrieval solution has been determined using the observations rather than the a priori information, and as such, the retrieval has provided new information about the actual state. Lastly, three indicators of the usefulness of the measurements for performing the retrieval can be derived from the singular values (λ_i) of the error-weighted weighting function matrix

$$\tilde{\mathbf{K}} = \mathbf{S}_\mathbf{y}^{-1/2}\mathbf{K}\mathbf{S}_\mathbf{a}^{1/2} \tag{11}$$

defined by *Rodgers* [2000]. The first of these indicators is the number of degrees of freedom for signal

$$d_s = \sum_i \frac{\lambda_i^2}{1+\lambda_i^2}, \tag{12}$$

which indicates the number of useful independent observations in the retrieval. Second, a count of the number of singular values greater than 1 (r_y) indicates the number of useful independent quantities retrieved from **y**. If less than the dimension of **x**, the ratio between the two identifies the fraction of **x** determined solely by the measurement. Finally, the Shannon information content

$$H = \frac{1}{2}\sum_i \ln\left(1+\lambda_i^2\right) \tag{13}$$

identifies the number of distinct states that can be determined as a result of **y** relative to the a priori information alone. If new elements are added to **y**, the change in H indicates how many more distinct states can be retrieved, thus quantifying the extent to which those observations improve knowledge of the state. Alternatively, changes in H can be used to evaluate the performance of a particular retrieval implementation over time for a single instrument (i.e., from one measurement to another, from day to day, and over longer time periods), or to compare the performance of multiple instruments in different locations, such as across a network.

2.4. Cloud-Screening Methodology

[18] Prior to application of the retrieval, cloud-contaminated field campaign measurements were removed from the data set so as to not misinterpret the effect of cloud cover as due to aerosols. This was accomplished by a program implementing the technique of *Long et al.* [1999] and detailed by *Long and Gaustad* [2004], which estimates fractional cloud coverage from ground-based broadband irradiance measurements. Since broadband data is not provided by the UV-MFRSR, results of the cloud-screening method based on open channel (i.e., unfiltered) measurements of a visible-wavelength MFRSR colocated at CENICA were obtained from the Pacific Northwest National Laboratory (PNNL). To account for discrepancies in the measurement intervals of the two instruments, cloud amounts were averaged over 3-min intervals to coincide with the UV-MFRSR data. However, the removal of all measurements for which the algorithm estimated a cloud fraction above 1% resulted in an overly sensitive screen that eliminated all but 38 measurements for the duration of the campaign. Since previous research has suggested that MFRSR retrievals of ω_{aer} may not require entirely cloud-

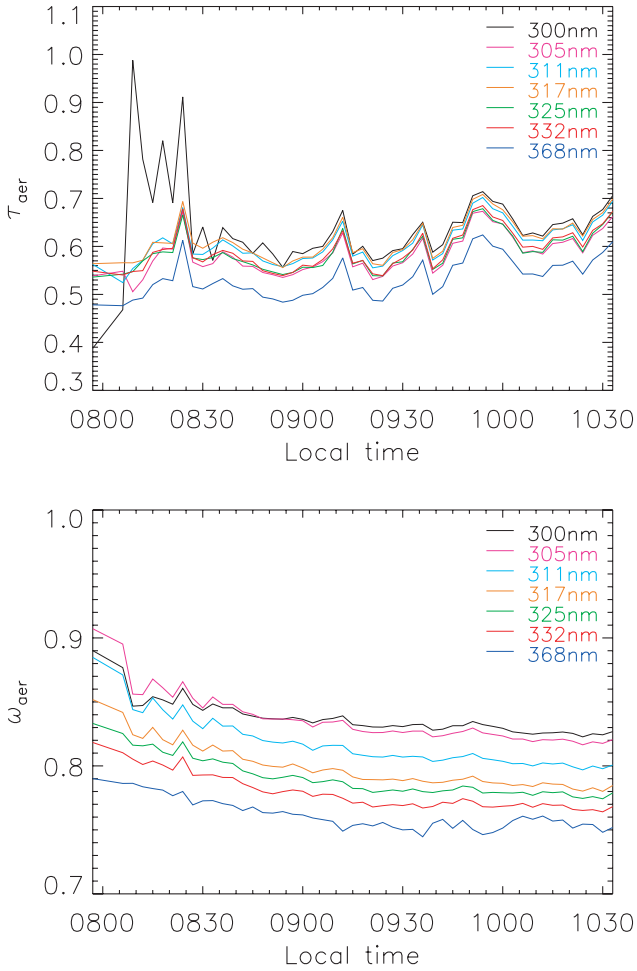

Figure 5. Time series of (top) τ_{aer} and (bottom) ω_{aer} retrieved in each passband for 15 April 2003 when correlations among the aerosol parameters are included in the a priori covariance matrix.

free conditions provided the direct solar beam is unblocked [*Krotkov et al.*, 2003], averaged cloud fractions of up to 2% were allowed to obtain a total of 455 measurements with which to perform the retrieval technique. Table 2 lists the number of cloud-screened measurements available on each day of the campaign along with the corresponding range of indices (numbered from 0 to 454) within the data set.

3. Results and Discussion

3.1. Retrieval Results

[19] Retrievals for each of the cloud-screened measurements were performed using the a priori state vector and variances summarized in Table 3. The range in ozone amounts was chosen based on TOMS measurements over Mexico City during April 2003 and field campaign values determined using the direct-Sun method [*Gao et al.*, 2001]. Similarly, the range in τ_{aer} was chosen based on Langley-derived results using the field campaign data, while ω_{aer} limits were selected based on prior research. Error variances assigned to $\mathbf{S_a}$ were assumed to follow a Gaussian distribution and calculated so as to achieve a 99.7% confidence interval corresponding to three standard deviations. Preliminary testing of the technique showed that the use of a lesser confidence interval allowed for unphysical retrieval results (e.g., $\omega_{aer} > 1$) while the use of a greater confidence interval was overly restrictive and resulted a retrieval solution essentially matching the initial guess. For consistency, the same Gaussian assumption and confidence interval were used in specifying a combined 10% measurement and model error in $\mathbf{S_y}$. While this percentage likely overestimates the error in the measurement alone, it was chosen as a crude estimate to include the uncertainties associated with modeling direct and diffuse irradiances, such as from aerosol composition and approximations in the radiative transfer method. A more rigorous determination of model and measurement error, as would be needed operationally, is the subject of ongoing research and beyond the scope of this work.

[20] At each retrieval, the off-diagonal elements in both $\mathbf{S_a}$ and $\mathbf{S_y}$ were set to zero, equivalent to assuming that all measurements and state vector parameters are uncorrelated. In reality, it is likely that correlations do exist among the τ_{aer} and ω_{aer} at the wavelengths of the UV-MFRSR and that forward model errors influencing more than one wavelength cause uncertainties in $\mathbf{S_y}$ to also be correlated. To illustrate

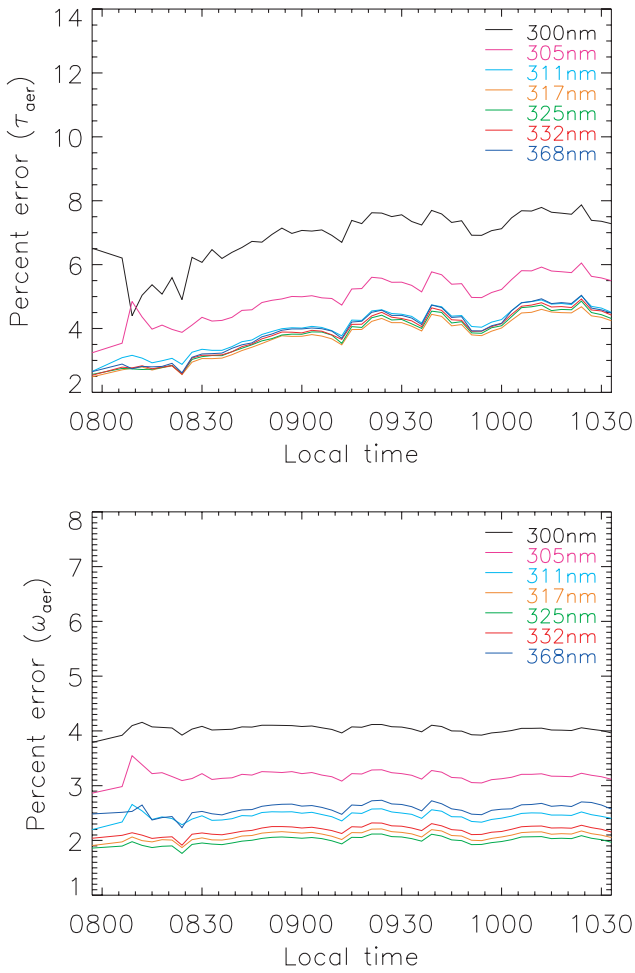

Figure 6. Time series of error percentages corresponding to one standard deviation in (top) τ_{aer} and (bottom) ω_{aer} for 15 April 2003 when correlations among the aerosol parameters are included in the a priori covariance matrix.

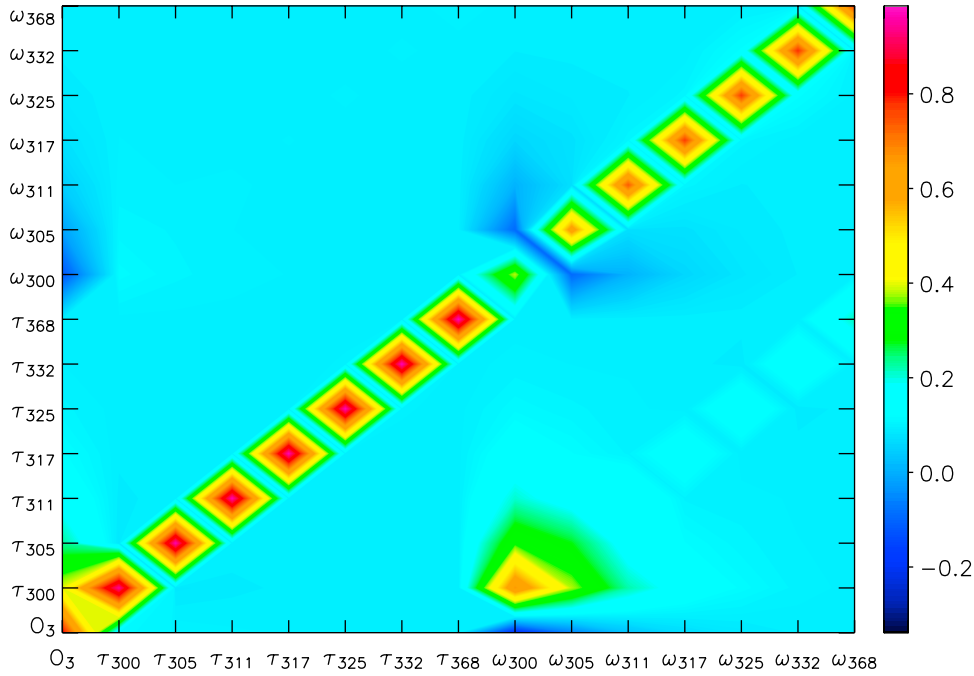

Figure 7. Depiction of the averaging kernel matrix for the 27 April 2003 retrieval at local noon. Peaks along the diagonal indicate resolution of the corresponding parameters based upon the measurements. Off-diagonal peak corresponding to ω_{aer} at 300 nm indicates poor resolution due to reliance upon a priori information.

the effect of this assumption on the retrieval outcome, rough correlations in $\mathbf{S_a}$ were used in a second set of retrievals for a subset of the field campaign data. It is important to note, however, that the use of improperly estimated correlations introduces the risk of adding spurious information into the retrieval that may, in fact, degrade the results. As such, a more precise determination of these correlations is needed for operational use.

[21] Table 4 summarizes the range of each parameter retrieved over the course of the campaign and the range in uncertainties corresponding to one standard deviation. Daily column ozone amounts were determined by averaging the ozone retrievals corresponding to individual measurements on each day. The range of ω_{aer} retrieved at each wavelength is similar to those obtained by *Petters et al.* [2003], who attributed absorption to the presence of black carbon aerosols. However, the latter found a distinct upward trend in the range of ω_{aer} with wavelength. To the contrary, Figures 2 and 3 illustrate a time series of τ_{aer}, ω_{aer}, and their associated errors from 15 April in which a downward trend in ω_{aer} (i.e., increasing absorption) with wavelength occurs. It is possible that this trend is the effect of an absorbing gas not accounted for in the model inputs, such as NO_2, which is associated with high levels of vehicle emissions as found in the MCMA and whose absorption cross sections increase with wavelength from 300 to 368 nm at 298 Kelvin [*Seinfeld and Pandis*, 1998]. To test this hypothesis, the sensitivity of the 15 April aerosol retrievals to NO_2 vertical column density

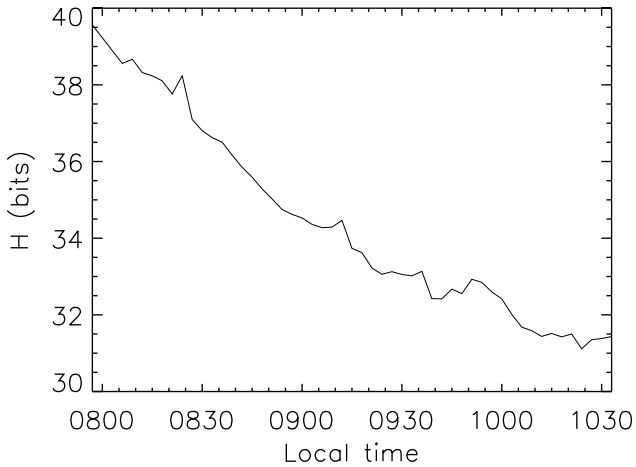

Figure 8. Time series of *H* in bits (converted from natural to base-two logarithm) corresponding to the optimal estimation retrievals on 15 April 2003.

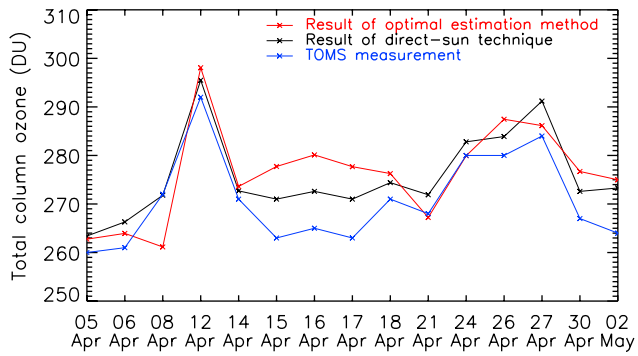

Figure 9. Comparison of daily column ozone amounts from optimal estimation results with Total Ozone Mapping Spectrometer measurements and the direct-Sun method.

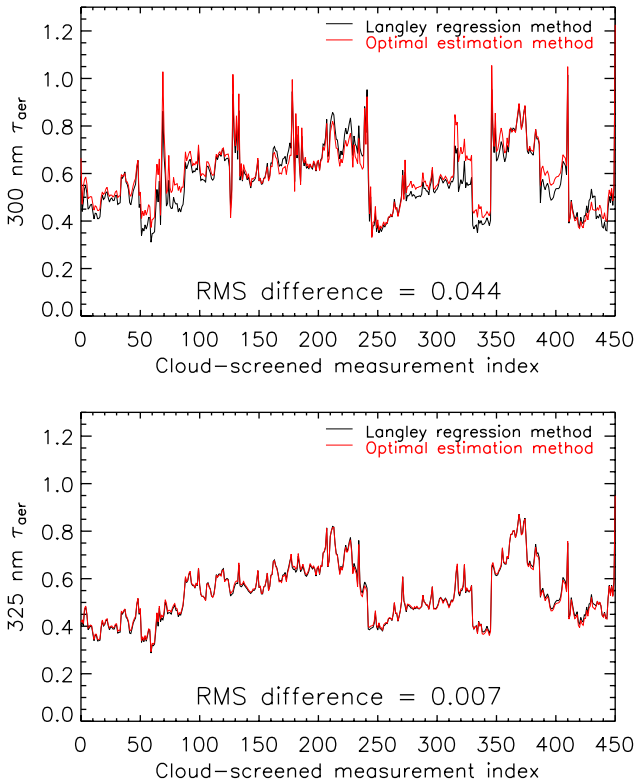

Figure 10. Chronological data series of τ_{aer} retrievals in the (top) 300 and (bottom) 325 nm passbands, for which agreement was worst and best, respectively, between the optimal estimation and Langley regression methods.

was studied. NO_2 densities were estimated for Mexico City based on differential optical absorption spectrometer (DOAS) surface measurements and lidar returns from the field campaign. Increasing the amount of NO_2 from 0 to 40 ppb within a morning mixing layer height of 840 m was found to raise ω_{aer} at 368 nm by 0.05 and lower τ_{aer} at the same wavelength by 0.04. Retrievals at shorter wavelengths were less affected. Thus the influence of NO_2 does not appear to be large enough to reverse the observed trend in ω_{aer}. Furthermore, these differences are generally of the same order of magnitude or less than the uncertainties in the retrieved τ_{aer} and ω_{aer} shown in Figure 3. (Recall that the curves in Figure 3 represent one standard deviation in each variable; hence even the large NO_2 effect at 368 nm falls within a 99.7% confidence interval determined from $\hat{\mathbf{S}}$). This supports the assertion that the 10% measurement and model error estimate was sufficiently large to account for the effects of NO_2, even though those effects were not explicitly modeled in $\mathbf{S_y}$. At the same time, these results suggest that the effect of NO_2 should either be modeled or retrieved in order for the algorithm to be used operationally, particularly in polluted regions where NO_2 is highly concentrated.

[22] As previously mentioned, the typical range in chemical composition of aerosol particles is likely to impose correlations in both τ_{aer} and ω_{aer} at the wavelengths of the UV-MFRSR. A benefit of the optimal estimation technique is the ability to model such correlations. By using (9) to construct a correlation matrix from the elements of $\hat{\mathbf{S}}$, correlations in the retrieval result are placed within a range from 1.0 (perfectly correlated) to −1.0 (perfectly anticorrelated). Figure 4 depicts an averaged correlation matrix for the 51 retrievals on 15 April in which the diagonal elements have been set to zero for greater emphasis of the off-diagonal elements. Positive correlations (shades of red) are evident for both τ_{aer} and ω_{aer} among neighboring wavelengths, particularly at 300 and 305 nm. Negative correlations (shades of blue) appear between τ_{aer} and ω_{aer} together at the same wavelength, and to a lesser magnitude at neighboring wavelengths. Additional correlations are evident between the total column ozone and aerosol parameters at the shortest wavelengths. It is interesting to note that, in general, the largest retrieval errors also occur at the shortest wavelengths. This reflects the fact that the 300 and 305 nm channels exhibit the least sensitivity to the aerosol properties being retrieved, which forces the algorithm to look toward neighboring channels to provide the information it needs to constrain the solution.

[23] Because it is an adaptation of $\hat{\mathbf{S}}$, the correlation matrix indicates to what extent the information provided by the model and measurements about the retrieval parameters is correlated, not whether the physical parameters themselves are correlated. To illustrate the effect of physical correlations, the 15 April retrievals were repeated with nonzero off-diagonal elements included in $\mathbf{S_a}$. For simplicity, aerosol parameters were assigned a perfect correlation with the other parameters of the same type, less 10% for every 6 nm change in wavelength. Cross correlations between τ_{aer} and ω_{aer} were excluded, as were correlations with column ozone. Figures 5 and 6 illustrate the resulting time series of τ_{aer}, ω_{aer}, and their associated errors, for comparison with Figures 2 and 3. Most notable in these figures are the ω_{aer} series at 300 and 305 nm, which conform more closely to the trend at middle and upper wavelengths, and the spectral trend in ω_{aer}, which is more distinct. In addition, retrieval errors in both τ_{aer} and ω_{aer} at 300 nm are reduced by nearly one third, going from 5–6% in the absence of correlations to 3–4% with them. This is a direct result of the fact that the imposed correlations between parameters allows the algorithm to use the observations at longer wavelengths, which exhibit greater sensi-

Table 5. Minimum and Maximum Root-Mean-Square (RMS) Differences in τ_{aer} Retrieved Using Optimal Estimation Versus the Langley Regression Method

	Passband						
	300 nm	305 nm	311 nm	317 nm	325 nm	332 nm	368 nm
Minimum daily RMS difference	0.019	0.005	0.002	0.003	0.004	0.004	0.003
Maximum daily RMS difference	0.116	0.040	0.026	0.016	0.015	0.020	0.027

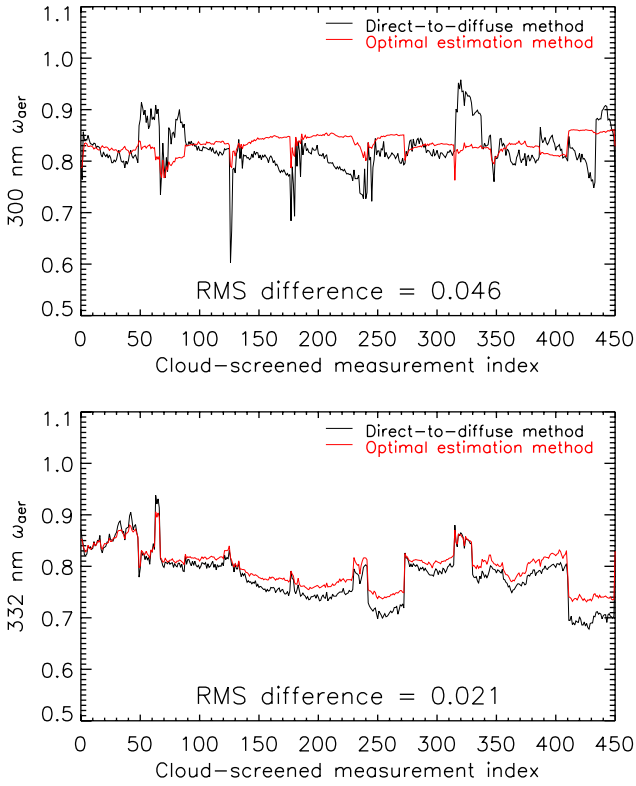

Figure 11. Chronological data series of ω_{aer} retrievals in the (top) 300 and (bottom) 332 nm passbands, for which agreement was worst and best, respectively, between the optimal estimation and direct-to-diffuse ratio methods.

tivity, to augment the lesser sensitivity at 300 nm. Laboratory experiments to better estimate the strengths of these correlations will have the potential to further improve the retrieval accuracy.

[24] To more completely examine the behavior and performance of the retrieval, the information diagnostics introduced in section 2.3 were applied. The field campaign mean value of d_s was determined to be 12.38, indicating that 88% of the observations assembled into **y** were independent of one another on average. The mean value of r_y was determined to be 14, which, although equivalent to the total number of singular values λ_i, is less than the dimension of **x**. This result indicates that the retrieval was generally underdetermined by 7% and is consistent with the averaging kernel matrix depicted in Figure 7. Peaks occurring along the diagonal of **A** with numerical values near 1 indicate that, for most retrieval parameters, the solution was resolved based upon the measurements. However, the off-diagonal peak corresponding to ω_{aer} at 300 nm indicates poor resolution due to reliance upon the a priori information and the determination of τ_{aer} at the same wavelength. Last, Figure 8 illustrates a time series of H corresponding to the retrievals on 15 April, in which H declines from a value of 39.6 bits prior to 0800 to a value of 31.4 bits shortly after 1030. This is equivalent to stating that, at 0800, the measurements provided a resolution of $2^{39.6}$ or 833 trillion distinct retrievable states relative to the a priori information alone, versus 2.8 trillion distinct retrievable states at the later time. Thus the measurements provided considerably more information to the retrieval earlier in the day, while the diffuse component of the irradiance was dominant over the direct beam. Given that ω_{aer} at 300 nm was the least well resolved parameter and that the diffuse irradiance alone contributes to the determination of ω_{aer}, it is consistent that the measurement vector **y** containing both diffuse and direct irradiances provided the most information to the retrieval while the diffuse component was strongest relative to the direct component.

3.2. Comparison to Independent Methods

[25] Once the retrieval results were determined, they were compared to the results of independent, more widely used methods. Specifically, daily column ozone amounts were compared to TOMS measurements and results of the direct-Sun method [*Gao et al.*, 2001]. This comparison is illustrated in Figure 9. In general, the optimal estimation results compared to within 5% of the independent methods and followed the day-to-day trend. Exceptions on isolated days, such as on 8 April, are likely due to the small number of cloud-free observations available for performing the daily average, since the direct-Sun method is not constrained to a cloud-screened set of observations. The higher values and difference in trend from 15–17 April may reflect an effort by the optimal estimation technique to compensate for NO_2 absorption of UV via an increase in the amount of ozone, although an ozone retrieval sensitivity study for 15 April found only a modest decrease of 1.7 DU in response to an increase in NO_2 from 0 to 40 ppb.

[26] Next, retrievals of τ_{aer} were compared to results of the Langley regression method described in section 2.1. Figure 10 (top) illustrates the τ_{aer} series comparison at 300 nm, where agreement between methods was worst among the seven wavelengths, while Figure 10 (bottom) presents the comparison at 325 nm, where agreement was best. In both cases, the comparison was quite favorable, as indicated by the similar trends and root-mean-square (RMS) differences shown. Table 5 summarizes the maximum and minimum daily RMS differences between the results of the two methods at each wavelength as further evidence of the precision with which the results agreed.

Table 6. Minimum and Maximum RMS Differences in ω_{aer} Retrieved Using Optimal Estimation Versus the Direct-to-Diffuse Ratio Method

	Passband						
	300 nm	305 nm	311 nm	317 nm	325 nm	332 nm	368 nm
Minimum daily RMS difference	0.013	0.012	0.008	0.006	0.008	0.004	0.013
Maximum daily RMS difference	0.102	0.071	0.060	0.056	0.053	0.045	0.054

[27] Finally, retrievals of ω_{aer} were compared against those from a direct-to-diffuse irradiance ratio technique. In this case, TUV4.2 was modified to produce lookup tables consisting of τ_{aer}, ω_{aer}, solar zenith angle, and irradiance ratio, from which values of ω_{aer} at each wavelength were interpolated based on the Langley-derived τ_{aer}, solar zenith angle at the time of measurement, and observed direct-to-diffuse ratio. Figure 11 (top) illustrates the ω_{aer} series comparison at 300 nm, where agreement between methods was again worst among the seven wavelengths, while Figure 11 (bottom) presents the comparison at 332 nm, where agreement was best. Due to poor resolution of ω_{aer} at the shortest wavelengths as previously noted, the comparison was less favorable in the worst case than for the 300 nm optical depths. However, in the best case, the comparison was once again quite favorable, as evidenced by the trend similarity and RMS difference shown in Figure 11 (bottom). Further evidence of the favorable comparison at longer wavelengths is presented in Table 6, which summarizes the maximum and minimum daily RMS differences between the two methods.

3.3. Comparison to Measurements

[28] The optimal estimation technique is designed to tune the retrieval results to the observations and, in some cases, to the a priori information, depending on the uncertainties specified in $\mathbf{S_y}$ and $\mathbf{S_a}$. Therefore, to verify that the retrieval was performing as intended, field campaign measurements

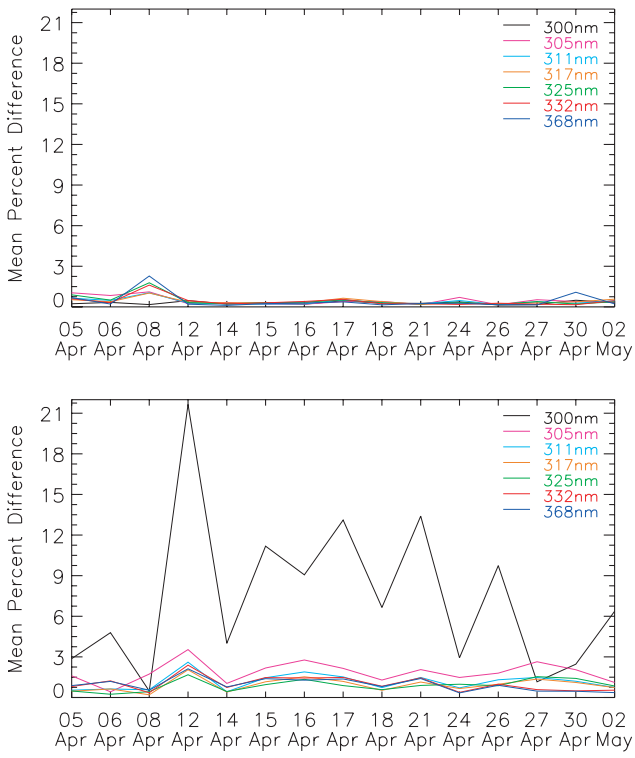

Figure 12. Daily mean percentage differences in direct normal irradiance simulated using (top) optimal estimation results and (bottom) results of the combined independent methods as model inputs relative to field campaign observations.

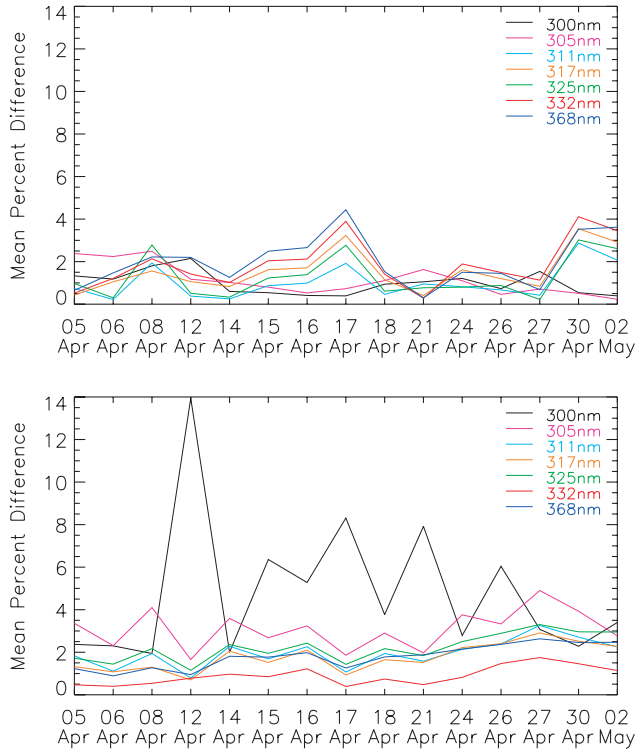

Figure 13. Daily mean percentage differences in diffuse horizontal irradiance simulated using (top) optimal estimation results and (bottom) results of the combined independent methods as model inputs relative to field campaign observations.

were compared to the irradiances simulated by TUV4.2 when using the retrieval results as inputs. As a point of reference, separate comparisons were used to examine the optimal estimation results and those from the combined independent methods. Figure 12 illustrates the daily mean percentage differences of the direct normal irradiance simulations relative to the observations in both cases, while Figure 13 illustrates the daily mean percentage differences relative to the diffuse horizontal measurements. The direct beam simulations compare favorably to the observations in every passband when using inputs from the optimal estimation technique, thus illustrating that the optimal estimation framework is capable of consistently and simultaneously matching with multiple measurements. Differences in simulated diffuse irradiance with respect to the observations were comparable between the retrieval methods in most cases, which is expected since ω_{aer} retrievals employed TUV4.2 in either case. In both the direct and diffuse cases, the actual differences between the irradiances that were measured and simulated from the optimal estimation results were considerably less than the assumed uncertainty percentage used to define $\mathbf{S_y}$.

[29] Finally, it is worth noting that differences in the retrieval results are not constant in time, as Figures 10 and 11 indicate. Since these retrieval methods each respond differently to the surrounding environment, both the differences between methods and the differences relative to the measurements change as the environment itself changes. This is precisely why, when using the optimal estimation

technique, it is important to determine the retrieval covariance matrix $\hat{\mathbf{S}}$ at each retrieval.

4. Conclusions

[30] As a retrieval technique, optimal estimation offers a number of advantages by not only allowing for the simultaneous determination of multiple parameters but also providing a built-in estimate of the retrieval uncertainty and relatively simple mathematical extensions for the analysis of the usefulness of the measurements. Moreover, adaptation of the retrieval to new information sources or a change in retrieval parameters only requires modification to the definitions of the measurement and state vectors and the weighting function matrix $\mathbf{K}$, provided that the forward model remains computationally efficient. At the same time, certain improvements to the proposed implementation are needed in order for the technique to be applied operationally and are currently being researched. First, laboratory experiments are needed to better estimate the correlations between parameters in the initial guess $\mathbf{x_a}$. Doing so will reduce the amount of independence in the retrieval parameters, thereby allowing more of the retrieval solution to be determined by the measurements and preventing an underdetermined retrieval. Second, the use of irradiance ratios in the measurement vector $\mathbf{y}$, such as the diffuse fraction or direct-to-diffuse ratio, will remove the dependence upon instrument calibration and allow for the amount of measurement uncertainty to be reduced. Third, uncertainty in the forward model needs to be determined more precisely, as opposed to the broad percentage applied in this research. With these improvements, it is anticipated that the optimal estimation technique will facilitate the continuous retrieval of ozone amounts and aerosol optical properties across the USDA UVMRP network, in order to supply ground truth for satellite measurements and promote development of a climatology for future research.

[31] **Acknowledgments.** We thank Mario and Luisa Molina at MIT for organizing the field campaign from which the data for this research was obtained. We also thank Chris Kummerow and Richard Eykholt at Colorado State University for their insights and comments on this project. This research was supported by the Office of Biological and Environmental Research of the U.S. Department of Energy (DE-FG02-94ER61748) as part of the Atmospheric Radiation Measurement Program and by USDA/CSREES Grant 2003-34263-13509.

References

Austin, R., and G. Stephens (2001), Retrieval of stratus cloud microphysical parameters using millimeter-wave radar and visible optical depth in preparation for CloudSat, *J. Geophys. Res.*, *106*, 28,233–28,242.

Bigelow, D. S., J. R. Slusser, A. F. Beaubien, and J. H. Gibson (1998), The USDA Ultraviolet Radiation Monitoring Program, *Bull. Am. Meteorol. Soc.*, *79*, 601–615.

Castro, T., S. Madronich, S. Rivale, A. Muhlia, and B. Mar (2001), The influence of aerosols on photochemical smog in Mexico City, *Atmos. Environ.*, *35*, 1765–1772.

Cooper, S. J., T. S. L'Ecuyer, and G. L. Stephens (2003), The impact of explicit cloud boundary information on ice cloud microphysical property retrievals from infrared irradiances, *J. Geophys. Res.*, *108*(D3), 4107, doi:10.1029/2002JD002611.

Cullen, J. J., P. J. Neale, and M. P. Lesser (1992), Biological weighting function for the inhibition of phytoplankton photosynthesis by ultraviolet radiation, *Science*, *25*, 646–650.

Dickerson, R. R., S. Kondragunta, G. Stenchikov, K. L. Civerolo, B. G. Doddridge, and B. N. Holben (1997), The impact of aerosols on solar ultraviolet radiation and photochemical smog, *Science*, *278*, 827–830.

Dockery, D. W., and C. Pope (1994), Acute respiratory effects of particulate air pollution, *Annu. Rev. Public Health*, *15*, 107–132.

Engelen, R., and G. Stephens (1999), Characterization of water vapour retrievals from TOVS/HIRS and SSM/T-2 measurements, *Q. J. R. Meteorol. Soc.*, *125*, 331–351.

Environment Canada (1999), Summary science assessment document, in *National Ambient Air Quality Objectives for Ground-Level Ozone*, Fed. Prov. Working Group on Air Qual. Objectives and Guidelines, Ottawa, Ont., Can., July.

Estupiñán, J. G., M. H. Bergin, J. R. Slusser, and R. S. Meltzer (2001), Measurement of aerosol optical depths in the UV-A: A comparison between a USDA Yankee Environmental Systems UV-multifilter rotating shadowband radiometer and an EPA Brewer spectrophotometer, *Proc. SPIE Int. Soc. Opt. Eng.*, *4482*, 212–223.

Gao, W., J. R. Slusser, J. H. Gibson, G. Scott, D. S. Bigelow, J. Kerr, and B. McArthur (2001), Direct-Sun column ozone retrieval by the ultraviolet multifilter rotating shadow-band radiometer and comparison with those from Brewer and Dobson spectrophotometers, *Appl. Opt.*, *40*, 3149–3155.

Gao, W., Y. Zheng, J. R. Slusser, and G. Heisler (2002), Impact of enhanced ultraviolet-b irradiance on cotton yield and qualities, *Proc. SPIE Int. Soc. Opt. Eng.*, *4482*, 381–387.

Harrison, L. C., and J. J. Michalsky (1994), Objective algorithms for the retrieval of optical depths from ground-based measurements, *Appl. Opt.*, *33*, 5126–5132.

Herman, B. M., R. S. Browning, and J. J. DeLuisi (1975), Determination of the effective imaginary term of the complex refractive index of atmospheric dust by remote sensing: The diffuse-direct radiation method, *J. Atmos. Sci.*, *32*, 918–925.

Krewski, D., R. T. Burnett, M. S. Goldberg, B. Kristin Hoover, J. Siemiatycki, M. Jerrett, M. Abrahamowicz, and W. H. White (2003), Overview of the reanalysis of the Harvard six cities study and American Cancer Society study of particulate air pollution and mortality, *J. Toxicol. Environ. Health A*, *66*, 1507–1551.

Krotkov, N. A., P. K. Bhartia, J. R. Herman, J. R. Slusser, G. Scott, G. Labow, A. P. Vasilkov, T. Eck, O. Dubovik, and B. Holben (2003), Goddard UV aerosol absorption closure experiment, *Proc. SPIE Int. Soc. Opt. Eng.*, *5156*, 54–62.

Kylling, A. A., F. Bais, M. Blumthaler, J. Schreder, C. S. Zerefos, and E. Kosmodis (1998), Effect of aerosols on solar UV irradiances during the Photochemical Activity and Solar Ultraviolet Radiation campaign, *J. Geophys. Res.*, *103*, 26,051–26,060.

L'Ecuyer, T. S., and G. L. Stephens (2002), An estimation-based precipitation retrieval algorithm for attenuating radars, *J. Appl. Meteorol.*, *41*, 272–285.

Liou, K. N. (2002), *An Introduction to Atmospheric Radiation*, 583 pp., Elsevier, New York.

Long, C. N., and K. L. Gaustad (2004), The shortwave (SW) clear-sky detection and fitting algorithm: Algorithm operational details and explanations, *Tech. Rep. ARM TR-004*, Atmos. Rad. Meas. Program, Lamont, Okla.

Long, C. N., T. P. Ackerman, J. J. DeLuisi, and J. Augustine (1999), Estimation of fractional sky cover from broadband SW radiometer measurements, paper presented at 10th Conference on Atmospheric Radiation, Am. Meteorol. Soc., Madison, Wis., 28 June to 2 July.

Madronich, S. (1992), Implications of recent total atmospheric ozone measurements for biologically active ultraviolet radiation reaching the Earth's surface, *Geophys. Res. Lett.*, *19*, 37–40.

Madronich, S. (1993), The atmosphere and UV-B radiation at ground level, in *Environmental UV Photobiology*, pp. 1–35, Springer, New York.

McKee, D. J. (Ed.) (1994), *Tropospheric Ozone: Human Health and Agricultural Impacts*, 333 pp., Lewis Publishers, Boca Raton, Fla.

Miller, S., G. Stephens, C. Drummond, A. Heidinger, and P. Partain (2000), A multisensor diagnostic satellite cloud property retrieval scheme, *J. Geophys. Res.*, *105*, 19,955–19,971.

Petters, J. L., V. K. Saxena, J. R. Slusser, B. N. Wenny, and S. Madronich (2003), Aerosol single scattering albedo retrieved from measurements of surface UV irradiance and a radiative transfer model, *J. Geophys. Res.*, *108*(D9), 4288, doi:10.1029/2002JD002360.

Rodgers, C. D. (2000), *Inverse Methods for Atmospheric Sounding: Theory and Practice*, 238 pp., World Sci., Hackensack, N. J.

Seinfeld, J. H., and S. N. Pandis (1998), *Atmospheric Chemistry and Physics: From Air Pollution to Climate Change*, 1326 pp., John Wiley, Hoboken, N. J.

Shaw, G. E., J. A. Reagan, and B. M. Herman (1973), Investigations of atmospheric extinction using direct solar radiation measurements with a multiple wavelength radiometer, *J. Appl. Meteorol.*, *12*, 374–380.

Slusser, J. R., J. H. Gibson, D. S. Bigelow, D. Kolinski, W. Mou, G. Koenig, and A. F. Beaubien (1999), Comparison of column ozone retrievals by use of an UV multifilter rotating shadow-band radiometer

with those from Brewer and Dobson spectrophotometers, *Appl. Opt.*, *38*, 1543–1551.

Slusser, J. R., J. H. Gibson, D. S. Bigelow, D. Kolinski, P. Disterhoft, K. Lantz, and A. F. Beaubien (2000), Langley method of calibrating UV filter radiometers, *J. Geophys. Res.*, *105*, 4841–4849.

Slusser, J. R., N. Krotkov, W. Gao, J. R. Herman, G. Labow, and G. Scott (2001), Comparisons of USDA UV shadow-band irradiance measurements with TOMS satellite and DISORT model retrievals under all sky conditions, *Proc. SPIE Int. Soc. Opt. Eng.*, *4482*, 56–63.

Stamnes, K., S. Tsay, W. J. Wiscombe, and K. Jayaweera (1988), Numerically stable algorithm for discrete-ordinate-method radiative transfer in multiple scattering and emitting layered media, *Appl. Opt.*, *27*, 2502–2509.

Stephens, G. L. (1994), *Remote Sensing of the Lower Atmosphere*, 523 pp., Oxford Univ. Press, New York.

Toon, O. B., C. P. Mckay, and T. P. Ackerman (1989), Rapid calculation of radiative heating rates and photodissociation rates in inhomogeneous multiple scattering atmospheres, *J. Geophys. Res.*, *94*, 16,287–16,301.

Wenny, B. N., J. S. Schafer, J. J. DeLuisi, V. K. Saxena, W. F. Barnard, I. V. Petropavlovskikh, and A. J. Vergamini (1998), A study of regional aerosol radiative properties and effects on ultraviolet-B radiation, *J. Geophys. Res.*, *103*, 17,083–17,097.

Wenny, B. N., V. K. Saxena, and J. E. Frederick (2001), Aerosol optical depth measurements and their impact on surface levels of ultraviolet-B radiation, *J. Geophys. Res.*, *106*, 17,311–17,319.

Wetzel, M. A., G. E. Shaw, J. R. Slusser, R. D. Borys, and C. F. Cahill (2003), Physical, chemical, and ultraviolet radiative characteristics of aerosol in central Alaska, *J. Geophys. Res.*, *108*(D14), 4418, doi:10.1029/2002JD003208.

Zheng, Y., W. Gao, J. R. Slusser, R. H. Grant, and C. Wang (2002), Yield and yield formation of winter wheat in response to enhanced solar ultraviolet-b radiation, *Proc. SPIE Int. Soc. Opt. Eng.*, *4482*, 335–340.

J. C. Barnard, Pacific Northwest National Laboratory, POB 999 (MSN K9-30), Richland, WA 99352, USA.

J. Davis, G. Scott, and J. R. Slusser, U.S. Department of Agriculture UV-B Monitoring and Research Program, Natural Resource Ecology Laboratory, Colorado State University, Fort Collins, CO 80523, USA.

C. D. Goering, T. S. L'Ecuyer, and G. L. Stephens, Department of Atmospheric Science, Colorado State University, 1371 Campus Delivery, Fort Collins, CO 80523, USA. (cgoering@atmos.colostate.edu)

S. Madronich, Atmospheric Chemistry Division, National Center For Atmospheric Research, P.O. Box 3000, Boulder, CO 80307, USA.